PROCEEDINGS OF SPIE

SPIEDigitalLibrary.org/conference-proceedings-of-spie

Coincidence technique to study ion-induced electron emission from atomically thin materials

Niggas, Anna, Schwestka, Janine, Weichselbaum, David, Heller, René, Aumayr, Friedrich, et al.

Anna Niggas, Janine Schwestka, David Weichselbaum, René Heller, Friedrich Aumayr, Richard A. Wilhelm, "Coincidence technique to study ion-induced electron emission from atomically thin materials," Proc. SPIE 12131, Nanophotonics IX, 121310H (24 May 2022); doi: 10.1117/12.2624402

SPIE.

Event: SPIE Photonics Europe, 2022, Strasbourg, France

Coincidence technique to study ion-induced electron emission from atomically thin materials

Anna Niggas[1], Janine Schwestka[1], David Weichselbaum[1], René Heller[2], Friedrich Aumayr[1], and Richard A. Wilhelm[1]

[1]TU Wien, Institute of Applied Physics, Wiedner Hauptstraße 8-10/E134, 1040 Vienna, Austria

[2]Helmholtz-Zentrum Dresden-Rossendorf, Institute of Ion Beam Physics and Materials Research, 01328 Dresden, Germany

ABSTRACT

We introduce our multi-coincidence setup used to study the interaction of highly charged ions with atomically thin materials. Ions are transmitted through freestanding two-dimensional materials and detected charge separated on a position sensitive microchannel plate detector with delay line anode. Electrons emitted upon the interaction of the projectile with the target can be detected either using a silicon surface barrier detector or a hemispherical analyser in order to gain information on the number of emitted electrons and their energy distribution, respectively. All data is stored in a listmode file allowing to set filters (e.g., time of flight, charge states) post measurement to identify the origin of correlated ion-electron pairs, i.e. we can determine whether detected ions were transmitted solely through the two-dimensional material layer or through its support structure. Using this coincidence technique we can correlate specific charge exchange and ion stopping channels (i.e. energy deposition) with particular electron emission scenarios (yield and energy distribution).

Keywords: interatomic Coulombic decay, highly charged ion, de-excitation, coincidence, electron emission, 2D materials

1. INTRODUCTION

Two-dimensional (2D) materials have recently become very popular as their unique properties[1,2] combined with a monolayer thickness give promising prospects for future applications.[3–6] Also for fundamental research, e.g. with charged particles, 2D materials turned out to be a treasure trove: On the one hand, by tuning a transmitting projectile's velocity, one can limit its interaction time with the material to a few femtoseconds[7,8] permitting an indirect approach to study processes on the femtosecond timescale.[9] On the other hand, restricting the material thickness to one monolayer and thus a maximum of one scattering event also allows new insights into basic ion-solid interaction processes.[10]

By using 2D materials and studying the neutralisation dynamics of highly charged ions (HCIs), the bottle neck problem of ultrafast ion de-excitation has already been solved: the interatomic Coulombic decay (ICD),[11,12] a two-center Auger process, was found to be the dominant de-excitation channel in the neutralisation of HCIs.[13] Only by applying ICD model descriptions to this problem, experimentally found neutralisation times of a few femtoseconds[7,13] can be explained. Previous attempts using common intra-atomic Auger de-excitation failed in this respect.[14–16] In addition to high neutralisation rates, ICD also predicts the emission of many low-energy electrons,[17] i.e., a study of emitted electrons can help support this model. For atomically thin materials, however, this involves difficulties, because it is necessary to distinguish emitted particles from the 2D sample and its support structure, respectively. Therefore, we present here a coincidence technique to detect correlated pairs of emitted electrons and transmitted ions, so that we can study the primary interaction of a HCI with a monolayer material.

Further author information: (Send correspondence to A.N. and R.A.W.)
A.N.: niggas@iap.tuwien.ac.at, R.A.W.: wilhelm@iap.tuwien.ac.at

Nanophotonics IX, edited by David L. Andrews, Angus J. Bain, Jean-Michel Nunzi, Proc. of SPIE
Vol. 12131, 121310H · © 2022 SPIE · 0277-786X · doi: 10.1117/12.2624402

2. METHODS

We employ an ion beam spectrometer for transmission experiments of HCIs through freestanding 2D materials. The spectrometer is discussed in detail in Ref. 18, a short overview will be given here in the following supplemented with an in-depth discussion of the electronics used for data acquisition.

HCIs are produced by a Dreebit EBIS-A ion source,[19] charge state q selected by means of a Wien filter and extracted from the source. We continuously tune the kinetic energy up to 10 kV $\times q$, where for xenon $q = 1 - 44$. After a self-made seven segment electrostatic lens assembly including an einzel lens, a deceleration lens and two pairs of deflection plates (final beam diameter $\sim$ 1 mm) the ions are transmitted through freestanding 2D materials, where we can adjust impact angles from normal to grazing incidence with a 4-axis manipulator. Transmitted ions are then exit charge state separated using a horizontal slit in front of a pair of deflection plates. Finally after a total flight distance from the target of approximately 1.1 m, the projectiles impinge on a 2D position sensitive microchannel plate (MCP) detector with delay line anode (DLD40) from RoentDek[20] (cf. Figure 1). Horizontal and vertical position on the MCP can then be translated into ion scattering angle and charge state, respectively.[18] By usage of RoentDek's FT12TP signal decoupler and ATR-19 amplifier and timing module (including a constant fraction discriminator (CFD)) the ion signal is fed to a time to digital converter (TDC, model RoentDek TDC8HP) for further analysis using the CoboldPC software. This data acquisition establishes detection of the ions with a timing precision < 0.2 ns and a spatial resolution < 0.1 mm.[21]

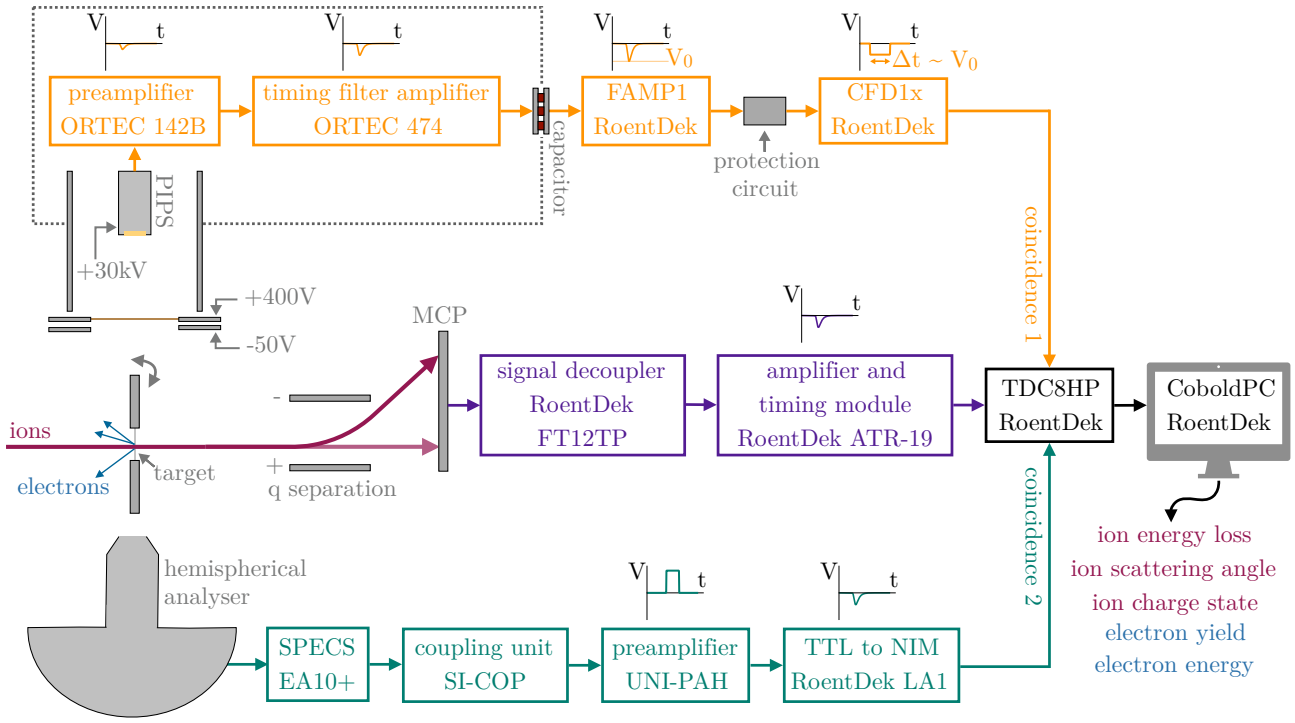

Figure 1. Schematic setup of our ion beam spectrometer. Ions are transmitted through a freestanding 2D material and are detected after the interaction charge separated on a position sensitive microchannel plate (MCP) detector with delay line anode. The MCP signal is then decoupled and amplified using RoentDek electronics and fed to a RoentDek timing to digital converter (TDC). Electrons emitted due to the ions' interaction with the target can be collected via two detectors: (1) A silicon surface barrier (PIPS) detector biased at $\sim$30 kV allows us to study the number of emitted electrons. The signal is amplified on high voltage and then transferred to ground potential using a set of capacitors. Further amplification is again performed using RoentDek electronics and the signal is then used as another input for the TDC. (2) A hemispherical analyser lets us analyse the energy of emitted electrons. Associated SPECS electronics deliver a TTL pulse that we convert to a NIM pulse necessary for the TDC. All TDC inputs (either (1) or (2) at the time) are then stored in a listmode file and can be evaluated using RoentDek's CoboldPC software.

To get information on the number of electrons emitted by a single ion impact, i.e. the electron yield γ, we use a surface barrier detector. In particular, our setup consists of a passivated implanted planar silicon (PIPS) detector commercially acquired from Canberra (PD100-13-100AM). The output signal is directly proportional to the energy deposited by impinging particles. Our detector is placed behind a grid biased at $\sim 400\,\mathrm{V}$ to attract all emitted electrons independent of their initial momentum. A negative potential ($\sim -50\,\mathrm{V}$) in front of the grid's frame ensures that the particles are not accelerated towards the solid border but the transparent grid. The detector itself is biased at 30 kV so that all electrons will be accelerated to the same energy and thus the PIPS' output signal is directly proportional to the number of emitted electrons ($U_{\mathrm{out}} \sim \gamma \times 30\,\mathrm{keV}$). For this reason the preamplifier (ORTEC 142B) and timing filter amplifier (ORTEC 474) are also biased at high voltage (dotted line in Figure 1) and we decouple the AC output pulse from the DC high voltage platform with a capacitor (HVP JX5T3M941K30KV). There, we take up the signal and further amplify it using a fast timing amplifier (RoentDek FAMP1) before we feed it to a CFD (RoentDek CFD1x), whose output then resembles the PIPS pulse's timing (rising edge) and pulse height (now pulse length). This final pulse serves then as another input for the TDC that reproduces the PIPS pulse height spectrum via a pulse length analysis: Primary pulses from the PIPS are amplified to 0-2 V what translates to pulse lengths with $\Delta t = 3.25\,\mathrm{ns/V}$ subsequently divided by the TDC over ~ 225 channels. Further we can determine the ion time of flight (TOF) with the PIPS as start and the MCP as stop trigger. To be precise, we need to consider two different TOFs: the electron TOF t_{electron} from the target to the PIPS depends on the electrostatic potential of the electron attraction grid and is in the order of $\sim$10 ns. In contrast, the ion TOF t_{ion} from the target to the MCP is in the order of $\sim 1\,\mu\mathrm{s}$ depending on the kinetic energy of the primary projectiles as well as their energy loss due to the interaction with the sample. What we measure here as TOF is the difference of ion TOF and electron TOF $t_{\mathrm{ion}} - t_{\mathrm{electron}}$, but since the latter is three orders of magnitude smaller than the ion TOF, this does not cause a major issue as long as TOFs are analysed only in terms of relative changes.

Another open question is the energy distribution of emitted electrons. Using the PIPS detector and an acceleration to 30 keV the electron energy is not accessible. A hemispherical energy analyser (HEA) is thus placed vis-à-vis of the PIPS. Since the HEA works only in field-free environments and the PIPS requires an attracting grid to collect all electrons, both detectors cannot be operated at the same time. A μ-metal shield around the target region and the HEA also prevents that external magnetic fields influence the electrons' trajectories. When using the HEA, several spectra need to be recorded - each for a certain electron energy - in order to receive a set of data points for a final energy distribution spectrum. A self-made LabVIEW VI[22] facilitates this process by changing HEA settings step by step and communicating with the CoboldPC software in order to start and stop measurements accordingly. The HEA (SPECS EA10+) is run in constant pass energy (190 eV) mode using its coupling unit (SI-COP) and preamplifier (UNI-PAH) as well as a TTL to NIM converter (RoentDek LA1) in order to provide a fast NIM pulse for the TDC. That way, we can again link transmitted ions and (now energy separated) electrons via the ion TOF. Please note, that for an analysis of the TOF it needs to be taken into account that the electron TOF t_{electron} varies with electron energy via the electron path length inside the HEA ($\sim 1\,\mathrm{m}$). Figure 2 shows TOF values for four different measurement series using xenon projectiles with 50 keV to 190 keV kinetic energy transmitted through single-layer graphene. For each ion energy, t_{ion} is constant, but decreasing t_{electron} with increasing electron energy lead to overall increasing TOFs $t_{\mathrm{ion}} - t_{\mathrm{electron}}$. Therefore, the data points can be well fitted using the equation denoted in Figure 2, where t_{ion} and d_e are fit parameters.

3. RESULTS

A schematic of our experiment geometry is depicted in Figure 3 panel **a**. The samples (here commercially acquired graphene samples from Graphenea[24]) generally consist of three layers: (1) gold TEM grid, (2) Quantifoil (amorphous carbon) support, and (3) 2D sample, e.g. single-layer graphene. For low- to medium-energy xenon ions, the TEM grid is not permeable as the grid's thickness is much thicker ($\sim 20\,\mu\mathrm{m}$) than the projected range in gold (14.5 nm for 100 keV Xe[25]). Ions going through the support ($\sim 10-20\,\mathrm{nm}$) and/or the 2D sample will be detected at the MCP. Hence in principal, all spectra show an aggregate of ions transmitting the freestanding 2D layer, support material, contaminated regions (or all three of them) as well as random noise from our detectors.[26] As examples, an exit charge state and an electron yield spectrum for 98 keV Xe^{30+} ions transmitted through single-layer graphene are shown in Figure 2 panels **b** and **c**, respectively. Whereas for the exit charge state we

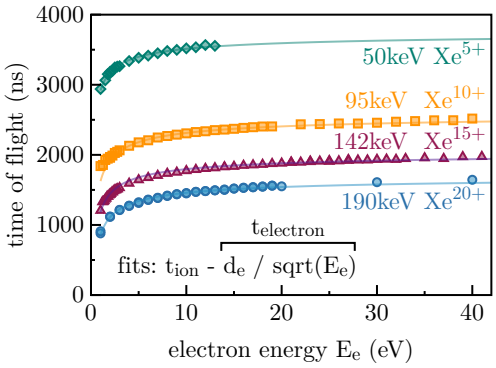

Figure 2. Time of flight (TOF) measurement. The measured time of flight represents the difference of ion TOF and electron TOF: $t_{\mathrm{ion}} - t_{\mathrm{electron}}$. As electrons with different energies have different flight times from the target to the HEA detector, the measured TOF increases with increasing electron energy (i.e. shorter electron TOFs). Here, data points are given for 190 keV Xe^{20+} (blue circles), 142 keV Xe^{15+} (red triangles), 95 keV Xe^{10+} (orange squares), and 50 keV Xe^{5+} (green diamonds) transmitted through single-layer graphene.

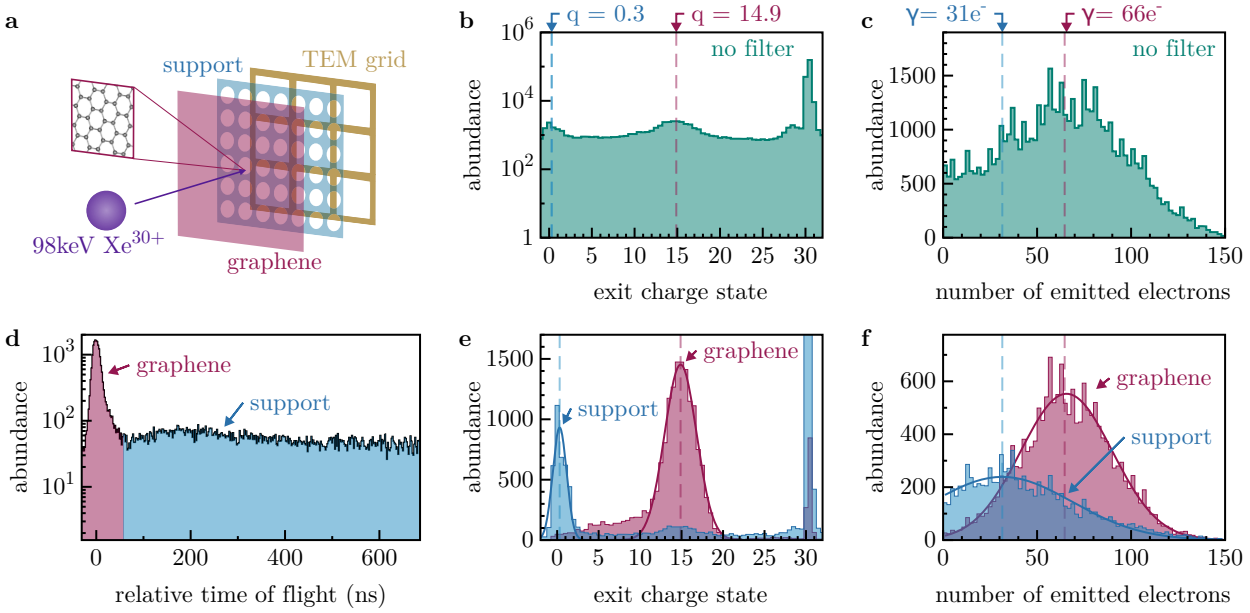

Figure 3. Charge exchange and electron yield. Panel **a** shows a schematic of our sample structure: 2D layers are placed on an amorphous carbon support structure based on a gold transmission electron microscopy (TEM) grid. Plain exit charge state (panel **b**) and electron yield (panel **c**) spectra represent a sum of all detected ions (transmitted through the 2D sample, the support, or both), electrons and noise. Using the ion time of flight (panel **d**) with the electron signal as start trigger as a filter we can however extract separate spectra for graphene and support both in regard of their charge exchange (panel **e**) and electron yield (panel **f**). All spectra are extracted from one single measurement using 98 keV Xe^{30+} ions as projectiles. The graphene layer was rendered using the software Vesta.[23]

can suspect two distributions at $q = 0.3$ and $q = 14.9$, for the electron yield no obvious (two) distributions can be picked out.

In order to distinguish these projectiles we consult the listmode files generated by our coincidence setup and have a look at the TOF (panel d): We find two distributions that we attribute to graphene (red) and the support (blue). The latter is located at longer TOFs since the ions deposit more energy in the 10-20 nm thick support than in single-layer graphene. We can now use these TOF regimes to filter exit charge state and electron yield

data, which results in the spectra given in panels **e** and **f**.

For the exit charge states, we can now clearly distinguish the two distributions we guessed from panel **b**. We find 15 captured electrons by the ions from graphene, whereas they completely neutralise while going through the much thicker support. This is consistent with our recent finding that the neutralisation depends on the time the ion interacts with a material.[8] Due to an overlap of the TOF peaks of graphene and support we cannot separate both contributions perfectly, which leads to small amounts of graphene/support counts in the respective other histogram. Ions detected with their incident charge state (here $q = 30$) stem from ions going through pores/holes in the sample without undergoing charge exchange processes as well as random coincidences with primary ions. Contrary to the unfiltered spectrum in panel **c**, in the TOF filtered electron yield spectrum in panel **f** we are able to determine mean numbers of emitted electrons: twice as many electrons are emitted by a single HCI impact from graphene (red) compared to the support (blue).[9,27]

At this point, it is noteworthy that all data presented in Figure 3 come from one single measurement using the PIPS detector and the MCP, i.e. the upper measurement branch shown in Figure 1. For electron energy determination this is more complex, because the HEA is only passable for electrons with a certain energy at a time. For each data point we here proceed as follows: In the exit charge state vs. scattering angle plot (Figure 4 panel **a**; 190 keV Xe^{20+} as projectiles) we define regions for the exit charge state distributions of the 2D sample (here graphene, red) and its support (blue). These distributions are either known from previous measurements[8,28] or can be verified using the PIPS as electron detector. As a next step, we filter the TOF (here with the HEA set to 3 eV electrons) using only the previously selected exit charge state/scattering angle combinations. The resulting TOF peaks can be seen in panel **b**. Again, we find longer TOFs on average for ions transmitted through the support compared to ions that went through the atomically thin graphene. The total sum of counts in these distributions, i.e. the integral, is now a measure of the abundance of electrons with the selected energy. The final electron energy spectrum is shown in panel **c**. Each data point is normalised to the number of incident ion counts on the detector in the graphene distribution. Since for the support we have rather bad statistic in the TOF peaks, no electron energy spectrum is shown in panel **c**. For graphene, we thereby find that the majority of emitted electrons is low-energetic (< 20 eV) in conformity with ICD. Two distributions can be distinguished at ~ 2 eV and ~ 9 eV, respectively. A detailed discussion of the electron energy distribution is, however, beyond the scope of this work and will be subject of a forthcoming publication.

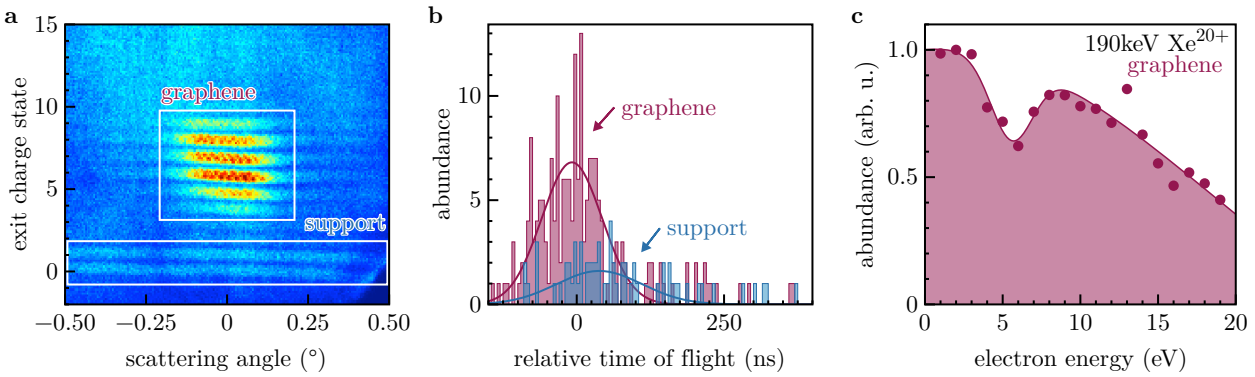

Figure 4. Electron energy. For each measurement point of an electron energy spectrum, we rely on the exit charge state spectrum (panel **a**) to select distributions previously identified using the procedure explained in Figure 3 (graphene: red, support: blue). Filtering for these regions leads to the time of flight distributions shown in panel **b**. The number of counts in these peaks (integral) represents the number of correlated electron-ion pairs that finally result in the energy spectrum in panel **c**, where a fit is added to guide the eye. For the support, the electron energy spectrum is very noisy due to the limited amount of correlated pairs (cf. panel **b**) and is thus not shown here. All data is taken from measurements using 190 keV Xe^{20+} ions and graphene as target. For panel **a** and **b** we used HEA transmission for 3 eV electrons.

4. CONCLUSION

We developed a multi-coincidence setup to study the interaction of highly charged ions and atomically thin materials. Therewith, we record the ion charge exchange, energy loss, and scattering angle together with correlated electrons with information on the electron yield and energy. Applying this technique for the model system of xenon ions transmitted through single-layer graphene we could show that a high number of electrons is emitted by one single ion impact[27] where the majority of electrons is low-energetic.[9] Both results are consistent with the prediction of the ICD model to the de-excitation of HCIs and support previous findings.[13,27]

ACKNOWLEDGMENTS

We thank Ulrike Diebold and Michael Schmid for their help with the HEA. Support by the Austrian Science Fund (FWF; projects Y 1174-N36 and I 4914-N) as well as TU Wien's Innovative Projects program and Doctoral College TU-D is gratefully acknowledged.

REFERENCES

[1] Novoselov, K. S., Geim, A. K., Morozov, S. V., Jiang, D., Zhang, Y., Dubonos, S. V., Grigorieva, I. V., and Firsov, A. A., "Electric field effect in atomically thin carbon films," *Science* **306**, 666 (2004).

[2] Miró, P., Audiffred, M., and Heine, T., "An atlas of two-dimensional materials," *Chem. Soc. Rev.* **43**, 6537 (2014).

[3] Peng, Y., Que, M., Tao, J., Wang, X., Lu, J., Hu, G., Wan, B., Xu, Q., and Pan, C., "Progress in piezotronic and piezo-phototronic effect of 2d materials," *2D Mater.* **5**, 042003 (2018).

[4] Feng, W., Jin, Z., Yuan, J., Zhang, J., Jia, S., Dong, L., Yoon, J., Zhou, L., Vajtai, R., Tour, J. M., et al., "A fast and zero-biased photodetector based on gate–inse vertical 2D p–n heterojunction," *2D Mater.* **5**, 025008 (2018).

[5] Novoselov, K., Mishchenko, A., Carvalho, A., and Neto, A. C., "2D materials and van der waals heterostructures," *Science* **353**, aac9439 (2016).

[6] Withers, F., Del Pozo-Zamudio, O., Mishchenko, A., Rooney, A., Gholinia, A., Watanabe, K., Taniguchi, T., Haigh, S., Geim, A., Tartakovskii, A., et al., "Light-emitting diodes by band-structure engineering in van der waals heterostructures," *Nat. Mater.* **14**, 301 (2015).

[7] Gruber, E., Wilhelm, R. A., Pétuya, R., Smejkal, V., Kozubek, R., Hierzenberger, A., Bayer, B. C., Aldazabal, I., Kazansky, A. K., Libisch, F., et al., "Ultrafast electronic response of graphene to a strong and localized electric field," *Nat. Commun.* **7**, 13948 (2016).

[8] Niggas, A., Creutzburg, S., Schwestka, J., Wöckinger, B., Gupta, T., Grande, P. L., Eder, D., Marques, J. P., Bayer, B. C., Aumayr, F., et al., "Peeling graphite layer by layer reveals the charge exchange dynamics of ions inside a solid," *Commun. Phys.* **4**, 180 (2021).

[9] Niggas, A., Schwestka, J., Balzer, K., Weichselbaum, D., Heller, R., Creutzburg, S., Inani, H., Tripathi, M., Speckmann, C., McEvoy, N., et al., "Ion-induced surface charge dynamics in freestanding monolayers of graphene and MoS_2 probed by the emission of electrons," *submitted* (2022).

[10] Creutzburg, S., Niggas, A., Weichselbaum, D., Grande, P., Aumayr, F., and Wilhelm, R., "Angle-dependent charge exchange and energy loss of slow highly charged ions in freestanding graphene," *Phys. Rev. A* **104**, 042806 (2021).

[11] Cederbaum, L. S., Zobeley, J., and Tarantelli, F., "Giant Intermolecular Decay and Fragmentation of Clusters," *Phys. Rev. Lett.* **79**, 4778–4781 (1997).

[12] Jahnke, T., Czasch, A., Schöffler, M. S., Schössler, S., Knapp, A., Käsz, M., Titze, J., Wimmer, C., Kreidi, K., Grisenti, R. E., Staudte, A., Jagutzki, O., Hergenhahn, U., Schmidt-Böcking, H., and Dörner, R., "Experimental Observation of Interatomic Coulombic Decay in Neon Dimers," *Phys. Rev. Lett.* **93**, 163401 (2004).

[13] Wilhelm, R. A., Gruber, E., Schwestka, J., Kozubek, R., Madeira, T. I., Marques, J. P., Kobus, J., Krasheninnikov, A. V., Schleberger, M., and Aumayr, F., "Interatomic coulombic decay: the mechanism for rapid deexcitation of hollow atoms," *Phys. Rev. Lett.* **119**, 103401 (2017).

[14] Herrmann, R., Cocke, C. L., Ullrich, J., Hagmann, S., Stoeckli, M., and Schmidt-Boecking, H., "Charge-state equilibration length of a highly charged ion inside a carbon solid," *Phys. Rev. A* **50**, 1435–1444 (1994).
[15] Winecki, S., Cocke, C. L., Fry, D., and Stöckli, M. P., "Neutralization and equilibration of highly charged argon ions at grazing incidence on a graphite surface," *Phys. Rev. A* **53**, 4228–4237 (1996).
[16] Hattass, M., Schenkel, T., Hamza, A., Barnes, A., Newman, M., McDonald, J., Niedermayr, T., Machicoane, G., and Schneider, D., "Charge equilibration time of slow, highly charged ions in solids," *Phys. Rev. Lett.* **82**, 4795 (1999).
[17] Jahnke, T., "Interatomic and intermolecular coulombic decay: the coming of age story," *J. Phys. B* **48**, 082001 (2015).
[18] Schwestka, J., Melinc, D., Heller, R., Niggas, A., Leonhartsberger, L., Winter, H., Facsko, S., Aumayr, F., and Wilhelm, R. A., "A versatile ion beam spectrometer for studies of ion interaction with 2D materials," *Rev. Sci. Instrum.* **89**, 085101 (2018).
[19] Zschornack, G., Kreller, M., Ovsyannikov, V. P., Grossman, F., Kentsch, U., Schmidt, M., Ullmann, F., and Heller, R., "Compact electron beam ion sources/traps: Review and prospects (invited)," *Rev. Sci. Instrum.* **79**, 02A703 (2008).
[20] RoentDek Handels GmbH, "Time and Position sensitive MCP Delay Line Detectors." https://www.http://roentdek.de. (Accessed: 8 February 2022).
[21] RoentDek Handels GmBH, "MCP Delay Line Detector Manual." http://www.roentdek.com/manuals/. (Accessed: 10 February 2022).
[22] National Instruments, "LabVIEW." https://www.ni.com/de-at/shop/software/products/labview.html. (Accessed: 10 February 2022).
[23] Momma, K. and Izumi, F., "VESTA 3 for three-dimensional visualization of crystal, volumetric and morphology data," *J. Appl. Crystallogr.* **44**, 1272–1276 (2011).
[24] Graphenea, "High quality Graphene producer - Graphenea." https://www.graphenea.com. (Accessed: 8 February 2022).
[25] Ziegler, J. F., Ziegler, M. D., and Biersack, J. P., "Srim–the stopping and range of ions in matter (2010)," *Nucl. Instrum. Methods Phys. Res. B* **268**, 1818–1823 (2010).
[26] Niggas, A., Schwestka, J., Creutzburg, S., Gupta, T., Eder, D., Bayer, B., Aumayr, F., and Wilhelm, R., "The role of contaminations in ion beam spectroscopy with freestanding 2D materials: A study on thermal treatment," *J. Chem. Phys.* **153**, 014702 (2020).
[27] Schwestka, J., Niggas, A., Creutzburg, S., Kozubek, R., Heller, R., Schleberger, M., Wilhelm, R. A., and Aumayr, F., "Charge-exchange-driven low-energy electron splash induced by heavy ion impact on condensed matter," *J. Phys. Chem. Lett.* **10**, 4805–4811 (2019).
[28] Creutzburg, S., Schwestka, J., Niggas, A., Inani, H., Tripathi, M., George, A., Heller, R., Kozubek, R., Madauß, L., McEvoy, N., et al., "Vanishing influence of the band gap on the charge exchange of slow highly charged ions in freestanding single-layer MoS_2," *Phys. Rev. B* **102**, 045408 (2020).